Progress in Organic Coatings 189 (2024) 108315

Contents lists available at ScienceDirect

Progress in Organic Coatings

journal homepage: www.elsevier.com/locate/porgcoat

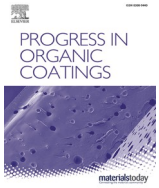

Hybrid aliphatic and aromatic diisocyanates forming mixed urea segments for high-performance polyurea

Khanisya Palaniandy [a], Sheik Ambarine Banon Auckloo [a], Giuseppe Cavallaro [b], Giuseppe Lazzara [b], Eng-Seng Chan [c], Pooria Pasbakhsh [a,*]

[a] Department of Mechanical Engineering, School of Engineering, Monash University Malaysia, Jalan Lagoon Selatan, Bandar Sunway, 47500 Subang Jaya, Malaysia
[b] Department of Physics and Chemistry "E. Segrè", University of Palermo, Viale delle Scienze, pad. 17, Palermo 90128, Italy
[c] Department of Chemical Engineering, School of Engineering, Monash University Malaysia, Jalan Lagoon Selatan, Bandar Sunway, 47500 Subang Jaya, Malaysia

ARTICLE INFO

Keywords:
Polyurea architectures
Diisocyanates
Microphase separations
Stress relaxations
Anti-corrosive coatings

ABSTRACT

Polyurea is gaining more traction in the realm of protective coatings on metal surfaces from corrosion. The properties of polyurea can be controlled by the judicious selection of its reactants. Herein, a series of polyurea based on hybrid aliphatic/aromatic diisocyanates are synthesized from isophorone diisocyanate (IP) and polycarbodiimide-modified diphenylmethane diisocyanate (ISO). The formulation composed of 37.5:62.5 (IP: ISO) weight ratio yields the highest tensile strength at 47.80 MPa, elongation at 500 %, and hardness of 95 HA. The findings are validated through field emission scanning and atomic force microscopic analysis, which reveals phase mixing surface and ductile fracture containing wide-ranging stretching lines due to enhanced resistance to deformation. Furthermore, synthesized polyureas present a unique stress relaxation pattern with gradual increase in stress under constant deformation, due to hydrogen bond reformation and dislocation creations during chain alignment. IP37.5-ISO62.5 demonstrates outstanding corrosion resistance after a 28-day exposure in salt spray test.

1. Introduction

Polyurea is a lightweight protective material which offers versatility in its application and exhibit excellent mechanical performance due to its viscoelastic behavior and unique dual-phase segmented microstructure [1–6]. Polyurea microstructure is made up of the hard (HS) and soft segments (SS) that form as a result of their thermodynamic incompatibility [7–9], which causes dual phase separation determined by factors such as the chemical structure of the precursors and the nature of the inter-facial region between the segments [10,11]. Due to this unique molecular structure, it imparts improved impact and blast resistance to its counterparts such as epoxy, polyurethane, and polysiloxane [12–14]. In recent years, polyurea has been studied for its corrosion protection efficiency and mechanical strength enhancer for coatings on pipelines [15,16], gas heaters [17,18] and marine composite cylinders [19,20].

Polymer coatings act as physical barrier for separating metal surface from corrosive agents through physiochemical mechanism [21], however, extreme environmental factors such as high salinity, strong ultraviolet (UV) or high temperature will lead to coating deterioration, blistering, or peeling affecting the performance of coated substrates [22]. In a study by Orlov [16], polyurea coatings were applied as retrofit coatings to protect existing underground pipeline of drinking water from corrosion. It was reported that, by applying the coating of 2–4 mm thickness, the service time of the lines could last up to 50 years [16]. Feng and Iroh [23] utilized aromatic polyurea in polyimide coating as mechanical property enhancer to protect 2024 aluminium in a 3.5 % NaCl solution. Their electrochemical impedance spectroscopy showed that the polyurea-b-polyimide coating containing 50 mol% of polyurea could last up to 8 years in the corrosive environment as a result of the enhancement of hydrogen bonding and increase in the degree of crystallinity in the matrix [23]. More recently, Huang et al. [19], had shown that polyurea as a reinforcer in epoxy improved the corrosion resistance by four times and wear resistance of the epoxy coating up to 73.2 %, thus providing a long-lasting protection in harsh environment.

Aromatic polyurea is derived from aromatic diisocyanates containing aromatic rings which provide high rigidity, maximum chemical stability and low reactivity [24]. Due to the rigidity, aromatic diisocyanate leads to significant microphase separation, which gives higher

* Corresponding author.
E-mail address: pooria.pasbakhsh@monash.edu (P. Pasbakhsh).

https://doi.org/10.1016/j.porgcoat.2024.108315
Received 26 November 2023; Received in revised form 24 January 2024; Accepted 5 February 2024
0300-9440/© 2024 The Authors. Published by Elsevier B.V. This is an open access article under the CC BY-NC-ND license (http://creativecommons.org/licenses/by-nc-nd/4.0/).

mechanical properties in the matrix. On the other hand, aliphatic polyurea is made using aliphatic diisocyanates which are kinetically mobile, less rigid and has better thermal degradation resistance [25]. Aliphatic based hard segments lead to better UV stability, hence making aliphatic polyurea ideal for topcoat of aromatic ones. The structure and orientation of diisocyanate molecules greatly impact the assembly of the hard segments and degree of phase separation which leads to variation in the mechanical properties [26–29]. Single diisocyanate-based polyurea have been extensively studied and such system itself yield a complex structure depending on the mobility and rigidity of the diisocyanate that impacts the intermolecular forces between urea chains [24].

Wilkes's group [26,30,31] investigated the effect of diisocyanate structure on the microstructural and mechanical properties of polyurea using a series of symmetric and asymmetric diisocyanates. They demonstrated that non-chain extended polyureas may well exhibit properties, such as the breadth of the service window, the average plateau modulus, stiffness, tensile strength, and elongation at break that are similar to chain extended segmented copolymers that possess distinctly higher hard segment content [26]. In a study on aromatic diisocyanates, they observed long-range ordering of hydrogen bonds between symmetrical 1,4-phenylene diisocyanate (PPDI) based urea groups, while kinked 1,3-phenylene diisocyanate (MPDI)-based urea groups did not display such behavior [30]. The formation of long-range connectivity of hydrogen bonds showed great importance in the formation of microphase-separated morphologies in the polyurea systems [30].

Li et al. [32] on the other hand, investigated the effect of two different aliphatic diisocyanates on the hard segmental packing of polyurea. They found that isophorone diisocyanate (IPDI) resulted in a looser hard segmental packing than linear aliphatic hexamethylene diisocyanate (HDI). IPDI has unstable cycloaliphatic ring that forms weak hydrogen bond while HDI is a linear chain that forms strong hydrogen bonds resulting in tight hard segmental packing [33]. IPDI-hard domains are loosely packed and easily penetrate the soft phase restricting the soft segment chains mobility, increasing the glass transition temperature (Tg) of soft phase. This hard segmental penetration would cause a less pronounced microphase separation or intermixed polyurea enhancing the HS/SS compatibility [34]. This penetration is advantageous for application of thermally responsive or self-healing materials. With application of temperature, the kinetic mobility of soft segmental chains increases and result in shorter stress relaxation time as evidenced by Li et al.'s study [32]. The incorporation of both aromatic and aliphatic diisocyanates imparts distinct advantages to the properties of polyurea. Consequently, relying on a single type of diisocyanate in polyurea formulation entails compromising the benefits offered by the other type and limiting its ability to be used as single layer coating system.

To date, polyurea has mostly been synthesized using single type of diisocyanate yielding either pure aliphatic polyurea or pure aromatic polyurea. There has been limited exploration into combining aromatic and aliphatic diisocyanate structures within a single polyurea matrix. Consequently, the resulting impact of hybrid diisocyanates, leading to the formation of two mixed hard segments, and their effect on the microphase separation of polyurea, remains unknown. This study aims to gain a thorough understanding of the underlying mechanisms governing the thermomechanical performance of polyurea derived from modified diphenyl methane diisocyanate (MDI) and IPDI, with varying concentrations. The focus is on the combination of an asymmetrical cycloaliphatic IPDI with a symmetrical modified MDI at the microscale, examining the effects on chain dynamics, segmental packing, and the distribution of hard and soft domains. As the first attempt to incorporate hybrid diisocyanates into a single polyurea matrix, this study exclusively investigates their influence on the final properties of polyurea, potentially paving the way for innovative designs in polyurea coatings for the industry.

2. Experimental

2.1. Materials

Aliphatic diisocyanate, Isophorone diisocyanate (IPDI) with 98 % purity was purchased from Sigma-Aldrich (M) Sdn. Bhd. Polycarbodiimide-modified diphenylmethane diisocyanate (Isonate™ 143 L) was purchased from Urethane. Polytetramethyleneoxide-di-p-aminobenzoate (P1000) with an average molecular weight of 1000 g/mol containing aromatic diamines from the VERSALINK® series was acquired from Evonik Industries. Sodium chloride salt, NaCl of 99.8 % purity analytical grade was purchased from Bendosen Laboratory Chemicals, Malaysia. All the materials were dried in a vacuum oven for 2 h to remove air cavitation and entrapped moisture before using.

2.2. Synthesis of mixed urea segment based polyurea

Table 1 lists the composition and tack-free times of all the films prepared in this study. Tack-free time is the time polyurea surface becomes non-sticky. The preparation method of IPx-ISOy is illustrated in Fig. 1. To prepare the isocyanate prepolymer mixture (Part A), Isonate™ 143 L and IPDI were weighed and mixed in a beaker using a stirrer. The mixture was then degassed in vacuum oven at room temperature to remove entrapped air bubbles. In another beaker, P1000 (Part B) was weighed and heated to 50 °C for 30 min to reduce its viscosity. The consistency of VERSALINK® P1000 at 50 °C is excellent to allow enough time for reaction when it is mixed with the isocyanates. Part A was poured into Part B and mixed until it is homogenous. Since this procedure is not performed under continuous vacuum, it is important to degas the polyurea mixture in vacuum oven before it is casted into 2 mm thickness film in a hard plastic mold. All the films were kept in a desiccator chamber with a relative humidity of 40 % and room temperature (~23 °C) for 7 days before they are tested. The bulk density of the films was measured on a density kit weighing balance. The films are labelled as IPx-ISOy such that x is the weight percentage of IPDI, and y is the weight percentage of Isonate 143 L in Part A composition. In this study, IP100-ISO0 is excluded as the film did not achieve tack-free or non-sticky state in 7 days.

2.3. Characterization of polyurea films

Fourier-transform infrared (FTIR) spectroscopy technique was employed using the FT-IR spectrometer to determine the chemical bonding present in the films with dimensions 10 mm × 10 mm × 2 mm. The FTIR program was set to collect 64 scans for absorbance versus wavenumber.

A monotonic uniaxial tensile test was carried out using Instron 5966 (10kN) Universal tensile machine for all films with a crosshead speed of 500 mm/min, both at room temperature (~23 °C). The films were cut into dumbbell shapes in accordance with ISO 37 type 2 using a pneumatic press. The test length of specimens is taken between the fixtures (25–30 mm). Three specimens were tested and the average tensile strength and average elongation at break values were recorded.

The hardness test was performed using a digital handheld Shore A durometer of range 0 ~ 100HA and five readings on different points of the films were taken and averaged. The values were determined within a few seconds once the reading stabilized.

The surface topography of selected films sized 1 cm × 1 cm × 2 mm was studied using an atomic force microscope (AFM) from Bruker, equipped with Nanoscope V controller and a MultiMode 8 head. The equipment was operated under air in ScanAsyst mode (automatic image optimization) using an etched silicon tip with a cantilever at a nominal spring constant of 225 N/m. AFM images (512 × 512) were recorded and estimated at room temperature with a scan rate of 1 Hz and a scan angle of 0° for a scan area of 10 μm × 10 μm. The average domain size is determined on ImageJ software by translating the AFM scan images to

Table 1
Composition of polyurea with varied amounts of different diisocyanates.

Film label	IP:ISO mass ratio	Overall composition (wt%)			Tack-free time (minutes)	Bulk density (g/cm^3)
		IP	ISO	P1000		
IP0-ISO100	0:100	0	30	70	32	1.182
IP25-ISO75	25:75	7.50	22.50	70	35	1.158
IP37.5-ISO62.5	37.5:62.5	11.25	18.75	70	38	1.093
IP50-ISO50	50:50	15	15	70	40	1.213
IP75-ISO25	75:25	22.50	7.50	70	65	1.015

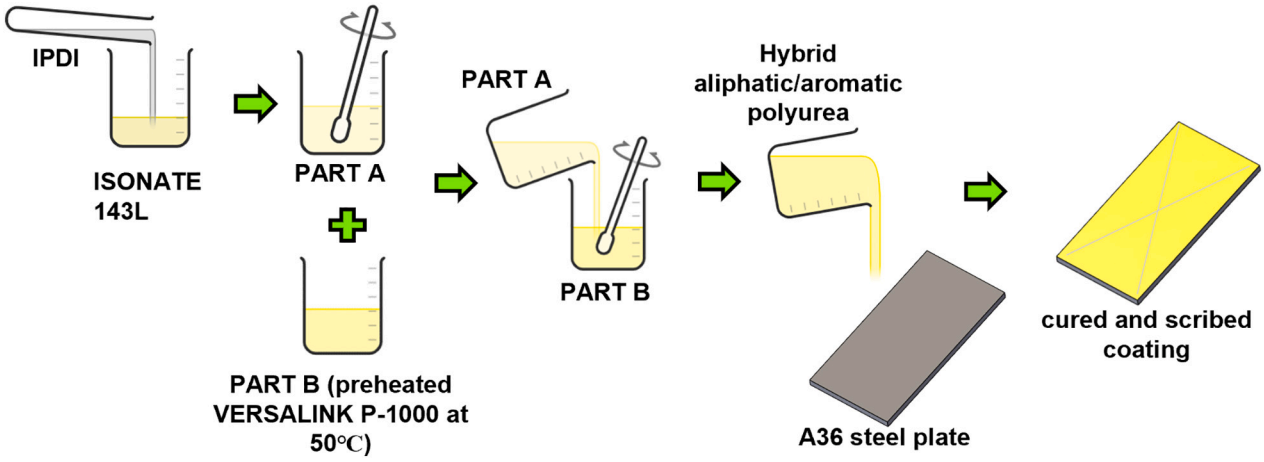

Fig. 1. Schematic illustration of IPx-ISOy polyurea solution preparation and coating application on mild carbon steel plate.

high/low contrast image.

To complement AFM observations, the tensile fracture surface morphology of selected films was examined under the field emission scanning electron microscope (FE-SEM) with an acceleration voltage of 5 kV. The specimens were pre-coated in a sputter coating machine using platinum to provide good conductivity.

Surface wettability of the films was tested using a laboratory setup water contact angle method. 10 μL deionized water was dispensed on the surface of specimen placed on a stage. A mounted high-resolution camera equipped with microlens is used to capture digital photographs of the water drop over a period of 4 min at every 30s intervals. The images were analyzed using Low Bond Asymmetric Drop Shape Analysis technique on ImageJ software [35]. The mean value of three contact-angle measurements was reported as the static contact angle. For the evaluation of surface free energy of polyurea films, two liquids with different polarities (water and N, N, dimethylformamide) were used on different locations of the samples. To calculate the overall surface free energy of polyurea, Eq. (1) was used, surface energy due to dispersive component and surface energy due to non-dispersive component were calculated using Eqs. (2) and (3), respectively.

$$\gamma_{IPx-ISOy} = \gamma^{d}_{IPx-ISOy} + \gamma^{p}_{IPx-ISOy} \quad (1)$$

$$\gamma_{L1}(1+cos\theta_1) = 2\left(\sqrt{\gamma^{d}_{L1}\gamma^{d}_{IPx-ISOy}} + \sqrt{\gamma^{p}_{L1}\gamma^{p}_{IPx-ISOy}}\right) \quad (2)$$

$$\gamma_{L2}(1+cos\theta_2) = 2\left(\sqrt{\gamma^{d}_{L2}\gamma^{d}_{IPx-ISOy}} + \sqrt{\gamma^{p}_{L2}\gamma^{p}_{IPx-ISOy}}\right) \quad (3)$$

The thermal degradation of IPx-ISOy was tested using thermogravimetric (TGA) analysis. The temperature range of each specimen (ca. 10 mg) was set to room temperature to 600 °C with a heating rate of 10 °C/min. A nitrogen flow was used during heating. Weight (%) and derivative weight (%/°C) data were collected over this temperature range.

The stress relaxation test was carried out under 3-point bending mode using a DMA Q800 apparatus (TA Instruments). A fixed deflection (0.5 % flexural strain) was applied to rectangular shaped specimens. Then, the stress vs time data were recorded. The experiments were carried out at 80 °C and 100 °C until the stress reached a plateau. It should be noted that 80 °C is being that it can be considered the curing temperature for polyureas. Moreover, the test was conducted also at 100 °C for the IP37.5-ISO62.5 sample to evaluate its suitability for high temperature applications.

Fatigue tests were carried out using Instron 5554 (100kN) machine under cyclic loading mode for IP0-ISO100, IP37.5-ISO62.5 and IP75-ISO25. The test was conducted to obtain S-N curves and the specimens were tested at different load values (10 %, 20 %, 40 %, 60 %, 80 % and 90 %) of the static failure load obtained from the tensile results. The fatigue experiment was conducted up to failure at a crosshead speed of 100 mm/min and at room temperature (~23 °C).

2.4. Application of mixed urea based polyurea coating on mild carbon steel

To evaluate the anti-corrosion performance, IP37.5-ISO62.5 was poured on ASTM A36 mild carbon steel plates as shown in Fig. 1. The steel plates with dimensions (50 × 25 × 3) mm were soaked in 5 wt% citric acid solution overnight and brushed to remove rust and impurities. They were air dried at 40 °C and the surface to be casted was cleaned using sandpaper grit 100 to achieve uniformity. Prior to casting, any remaining residual particles were wiped off using acetone. The initial mass and average thickness along each coupon were measured. IP37.5-ISO62.5 polyurea solution was poured on the steel plates to achieve thickness of 1 mm. After application, the freshly coated steel plates were left at room temperature for 7 days for full curing. The mass after coating and thickness along the plates were measured.

2.5. Assessment of corrosion properties of mixed urea based polyurea coating on mild carbon steel

The coating thickness was measured with a micrometer and the mass of steel plates were measured before and after coating application.

Anticorrosion performance was tested by neutral salt-spray (NSS) test chamber in accordance with ASTM B117. Before testing in the salt spray chamber, the cured plates were handled as follows: the cut edges and back surface were protected using an adhesive Scotch tape so that they do not get corroded. Then, in the middle part of each plate, a 'X' scribe with the length of 35 mm and 5 mm width was made through the coating using a sharp wooden chisel without touching the edges.

The scribed plates were placed on the racks at 45 degrees angle (slanted) to prevent accumulation of excess salt drips in the salt spray chamber leading to the accelerated onset of corrosion: 100 % rh, $T = 35\ ^{\circ}C$, pH = 7, continuous spraying of 3.5 % aqueous NaCl solution. The duration of the NSS test was set to 7, 14, 21 and 28 days of continuous exposure. Three plates were taken out periodically and dabbed with clean wipes and the wet masses were measured. Swelling percentage and hardness after exposure are determined. The visual appearance of corroded coatings for 14 and 28 days of exposure was studied under an optical microscope. The corrosion growth is calculated using Eq. (4).

$$R_d = \frac{1}{2}(d - d_0) \tag{4}$$

where d (mm) is the average width of the total of corrosion damage and d_0 (mm) is the scratch width before the test.

Although peel tests are commonly opted to compare the bond quality of coating to the substrate during its aging, in this study, the primary focus is on the effect of dual diisocyanates on the resulting properties of the films. The sole intention of coating the materials on steel substrates is to compare the quality of visual appearance of the coatings, hardness, swelling, post aging.

3. Results and discussion

3.1. Fourier transform infrared analysis

FTIR spectroscopy was used to determine if all the isocyanates have reacted in the polyurea leaving VOC-free samples. The FTIR spectra of IPx-ISOy presented in Fig. 2 show that all the films have similar characteristic peaks to typical polyurea and polyurethane structures. They did not show the stretching vibration band at 2270 cm^{-1} characteristic of the isocyanate free NCO group [7], which confirmed that all of the isocyanate groups reacted during the polymerization and curing. The peak at 3300 cm^{-1} is associated with hydrogen bonded NH stretching bonds. IP75-ISO25 experienced a left shift to wavenumber 3328 cm^{-1} at this peak indicating that the hydrogen bonded N—H bonds are more disordered in the matrix. They could either be bonded with neighboring urea group monotonically or exist by themselves. It is well known that the infrared absorbance of bidentate H-bonded urea carbonyl groups in ordered (crystalline) hard domains appears at lower wave number than that of H-bonded urea carbonyl groups in disordered (amorphous) domains [36–39]. High absorbance intensity was observed at wavenumber 1728 cm^{-1} for IP25-ISO75, IP37.5-ISO62.5 as compared to the rest of synthesized polyurea films indicating higher occurrence of ordered H-bonded carbonyl groups. The bending of NH and stretching of CO simultaneously in the urea linkage, NH-C═O molecule is observed at 1557 cm^{-1} [40]. The presence of all these aforementioned characteristic peaks confirms the formation of urea linkages in the prepared polyurea structures. The absence of free N—H_2 peak at 3500 cm^{-1} in all the films except for IP50-ISO50 and IP75-ISO25 (observation of a broad "bump") indicates that the phase mixing of hard and soft domains is dominant in these matrices [41]. This means that the phase separation is more dominant in IP50-ISO50 and IP75-ISO25 suggesting that the excess aliphatic diisocyanates favored the self-assembly of hard segments into hard phases [42]. The influence of the diisocyanate structure is not too apparent on the absorbance intensity of the peaks indicating that the characteristic bond formation is not sufficient for distinct detection via the FTIR spectroscopy.

3.2. Mechanical properties

Monotonic uniaxial tensile test was conducted at a high crosshead speed of 500 mm/min to evaluate the tensile properties of IPx-ISOy films. All the films exhibited typical elastomeric behavior as shown in Fig. 3(a). The stress-strain curves can be divided into three stages; stage

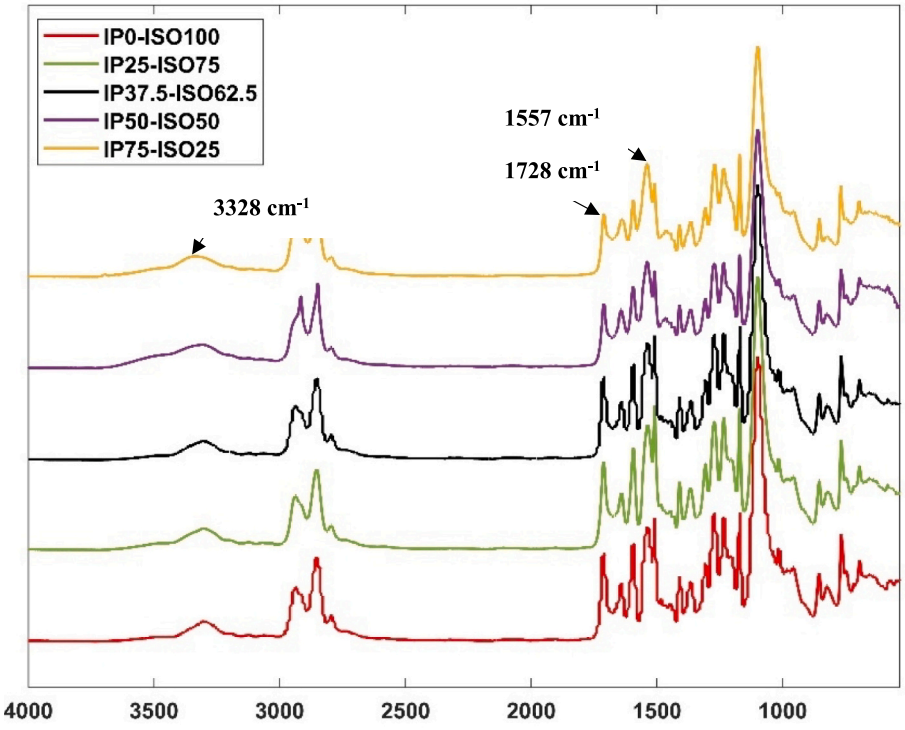

Fig. 2. Stacked FTIR spectra presenting absorbance versus wavenumber of IPx-ISOy with increasing amount of aliphatic diisocyanate (from bottom to top).

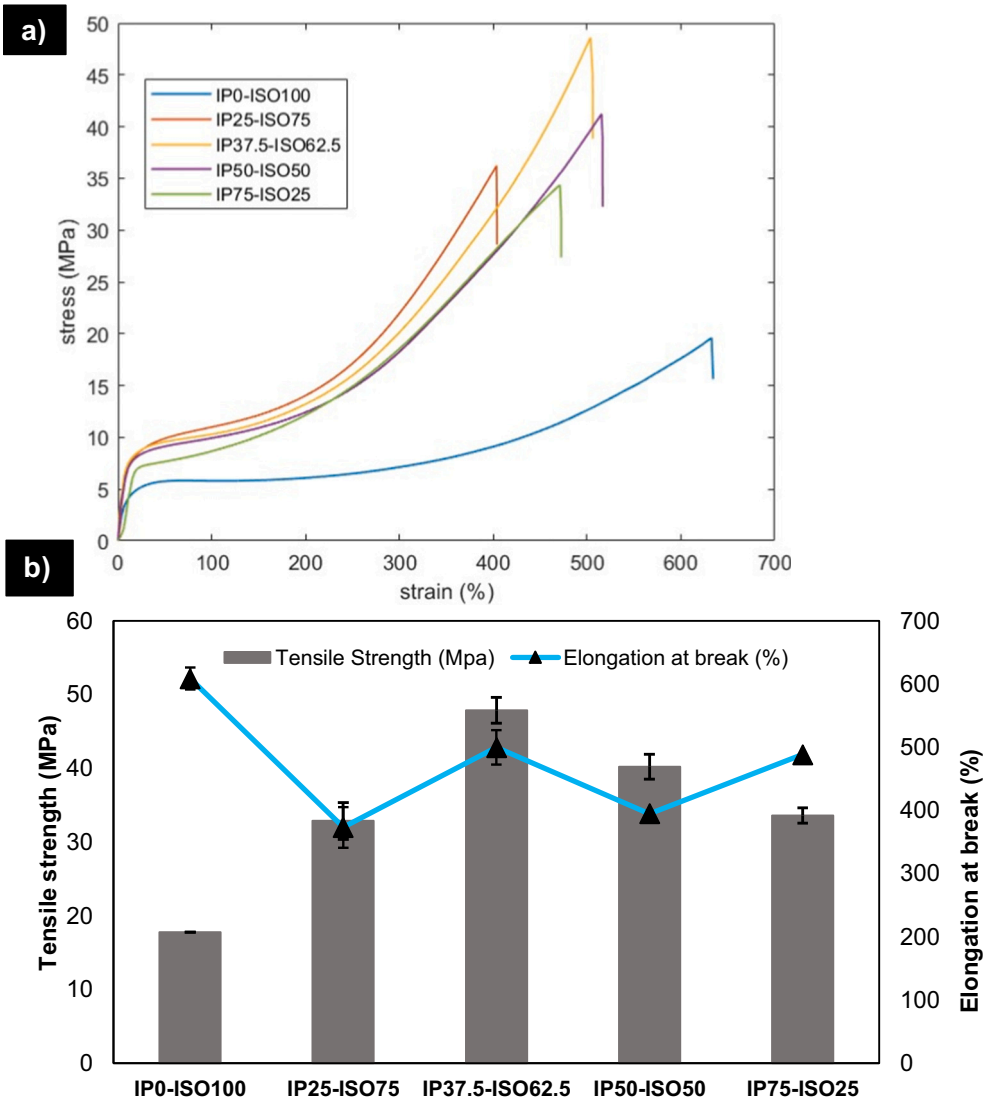

Fig. 3. Tensile test graphs of IPx-ISOy films. a) Comparison of monotonic tensile stress-strain curves of the best specimen at crosshead speed of 500 mm/min and b) bar chart of average failure strength and line graph of average elongation.

I: elastic deformation phase, stage II: strain hardening and plastic deformation phase (the largest phase) and stage III: failure point. In contrast to our previous work on pure aliphatic polyurea [7], the yield behavior of the present IPx-ISOy is less distinct (no occurrence of yield point or yield drop phenomenon) and transitioned smoothly into stage II, implying that the inclusion of aromatic diisocyanate speeds up the dynamic rearrangement of the hard segments during loading. A clear trend is noticeable in the gradient of stage I, where the modulus of elasticity is observed to have increased with the addition of aliphatic isocyanate reaching its peak at 37.5 wt% of IPDI and then declined slightly as shown in Table 2. Most importantly, the modulus of elasticity of IP75-ISO25 is still higher than that of IP0-ISO100, implying the aliphatic chains are creating mobile dislocations in the form of aliphatic hard segments, so they can resist greater elastic deformation. The increase in modulus can be influenced by possible $\pi - \pi$ interactions between adjacent aromatic moieties and hydrogen bonds between the N—H group in urea as well as the O group in urea and ether contributing to the rigidity of the hard domain [43]. Another suggestion is that higher concentration of aliphatic hard segments could create aggregates resulting in mixed urea hard segments (consisting of both hard and soft segments) across the matrix due to their proven mobile nature [26,44].

Fig. 3(b) displays the tensile strength and elongation at break pattern of IPx-ISOy, whereby the tensile strength increases with increasing IPDI content at constant concentration of amine oligomer and achieves a

Table 2
Average values of monotonic tensile test and hardness test with the corresponding statistical analysis data.

Films	0.2 % Offset Yield Strength (MPa)	Elastic modulus (MPa)	Tensile strength (MPa)	Elongation at break (%)	Hardness (HA)
IP0-ISO100	2.75 ± 0.11	62.50 ± 1.20	17.76 ± 1.24	608.93 ± 17.72	88.2 ± 3.3
IP25-ISO75	4.50 ± 0.05	87.10 ± 2.34	32.87 ± 2.50	373.20 ± 32.11	81.8 ± 1.4
IP37.5-ISO62.5	4.75 ± 0.04	178.57 ± 2.17	47.90 ± 1.76	499.94 ± 3.13	95.4 ± 1.5
IP50-ISO50	4.00 ± 0.02	108.82 ± 3.45	40.25 ± 1.69	394.88 ± 27.34	90.9 ± 0.7
IP75-ISO25	0.20 ± 0.01	99.67 ± 2.96	33.63 ± 1.03	488.37 ± 5.21	78.7 ± 2.5
p-Value	6.09×10^{-15}	1.11×10^{-12}	3.78×10^{-8}	1.68×10^{-8}	2.53×10^{-10}

maximum at 37.5 wt% IPDI, then declines at higher IPDI wt%. This implies that maximum crosslinking of adjacent urea moieties and maximum amount of ordered (bidentate) hydrogen bonding is occurring at IP37.5-ISO62.5. In IP0-ISO100, there is only one type of NCO carrier, which is the symmetrical and stable cyclic ring of MDI. As shown in Table 1, IP0-ISO100 has the shortest tack-free time due to the fast reactivity of the NCO aromatic cyclic rings with amine groups resulting in rapid formation of urea linkages [26]. This gives a direct effect on the elastic modulus whereby IP0-ISO100 exhibits the lowest value (62.50 MPa).

The trend of the elongation at break of IPx-ISOy films as observed from Fig. 3(b) appears to show a "zigzag" pattern. Maximum elongation is achieved by IP0-ISO100 at 608 %, and it decreased greatly with addition of 25 wt% IPDI but increased slightly to 500 % at the optimal IPDI amount and then again decreased with addition of 50 wt% IPDI, later increased with 75 wt% IPDI. The same trend is reproduced with different batches of IPx-ISOy samples which implies that there was no error occurred in the making of these samples. Thus, the "zigzag" trend has to be due to the combination of IPDI and MDI at different mass ratios and their effect on the type of hydrogen bonding between the urea groups in the chain and the consequent chain alignment behavior during tensile loading. At this juncture, it is worth to conclude that the tensile strength of polyurea has no direct correlation to the elongation at break of polyurea. It is the backbone chemistry of polyurea that influences all the tensile properties of polyurea, and these properties are independent of each other.

Shore A hardness test determines the influence of diisocyanate structure on the resistance of IPx-ISOy films to permanent indentation. Hardness value can reflect the bonding strength and cohesive ability of the dual segmented matrix [45]. The Shore A hardness of IPx-ISOy films is higher than recent studies reported on polyurea's hardness in the literature [45–48]. The hardness is the highest at 37.5 wt% IPDI, however, the hardness of IP0-ISO100 is found to be higher than the hardness of IP75-ISO25. In other words, IP75-ISO25 is a softer film than IP0-ISO100. The hardness of IPx/ISOy increased with increasing IP concentration up to 37.5 wt% due to increase in crosslinking polymerization via hydrogen bonding. The flexible nature of cycloaliphatic IPDI possessing high steric hindrance due to the three methylene (-CH_3) group attached to the cyclic ring [49,50]. The effect reduces the reactivity and slows down isocyanation reaction, taking its time to adopt spatial orientation for hydrogen bonding. At the same time, it is known that the hard segments assemble and connect to each other via formation of hard domains. The slow reaction and the assembly could improve the cohesive forces between the chains and the domains. A study by Mudri et al. [51] comparing the effect of aromatic and cycloaliphatic isocyanate on the hardness of polyurethane acrylate also showed that IPDI based polymer had higher hardness than TDI based ones. From the hardness result, we can see that the resulting hard segments made from both aliphatic and aromatic diisocyanates increased the cohesive forces via covalent bonding. These hard segments may have interacted with each other via strong hydrogen bonding between adjacent polyurea chains. However, when the concentration of IPDI surpasses the optimal value, the cohesiveness of the hard segmental chains is weakened.

From the tensile and hardness tests of IPx-ISOy, it could be seen that the ideal amount of IPDI in this mixture seems to be 37.5 wt%. Naturally, aliphatic diisocyanates are kinetically mobile and IPDI being a loosely bulk structure takes greater space coverage in the matrix as compared to MDI. The inclusion of them at smaller amount ($\leq$37.5 wt%) indicated that they were involved significantly in the formation of hydrogen bonding between the urea groups in the chain. When it is added beyond its optimal amount, it becomes saturated in the matrix, resulting in them existing as loose hard segments taking greater space in the matrix which makes them resist lesser to deformation. The high steric hindrance of IPDI could eventually help to slow down the gelling of polyurea [7]. This means that, their inclusion allows the isocyanates from aromatic and aliphatic to slowly rearrange themselves in a more synchronized manner positioning the hard segments and soft segments equally throughout the matrix. On the contrary, the aromatic ring is far more rapid and competitive dynamically, thus adding more aliphatic isocyanates reduces their resistance to deformation and indentation. However, with increasing amount of aliphatic isocyanates, rate of energy absorbed by polyurea during loading increased significantly as observed from the difference in the area under the curve of the stage II region in the stress-strain curves. Another advantage of having steric hindrance is that it reduces unwanted side reaction, which in this case the most obvious reaction between free NCO with moisture in the air producing CO_2 [52,53]. Instead, the isocyanate prepolymer chains and polyamine chains direct themselves to react together. During the solution preparation, it was very much evident that with increasing amount of aliphatic isocyanates, there were lesser bubbles formed in the solution. All the tensile properties and hardness values passed the one-way ANOVA statistical test with 95 % confidence. It is worth noting that each of the IPx-ISOy films exhibited significantly different tensile and hardness results and achieved a p-value of <0.05 as displayed in Table 2.

3.3. Surface topography and morphology

To delve into the dependence of aliphatic diisocyanate content on the microstructure of polyurea, AFM imaging was conducted on the surface of as cast IP0-ISO100, IP37.5-ISO62.5 and IP75-ISO25. Fig. 4(a, c, e) are the AFM height images while Fig. 4(b, d, f) are the AFM phase images. From the height images, we could see that the height range of IP0-ISO100 is the greatest followed by IP75-ISO25 and then IP37.5-ISO62.5, implying that the surface of IP0-ISO100 contains the most defects which could be caused by CO_2 bubbles or uneven solution casting.

The phase imaging on the other hand presents a clearer contrast as compared to the height images. In previous works on polyurea and polyurethanes [54,55], it was reported that the brighter regions in the phase imaging, attribute to the hard domains and darker regions to the soft domains. Fig. 4(b, d, f) shows two types of phase contrast: a bright, featureless matrix and dark elements of different size dispersed in this matrix. We attribute this to images of the dispersed phase, rich in hard segments, which appear on the microscale structural level. IP37.5-ISO62.5 and IP0-ISO100 both exhibit mixed phase morphology (Fig. 4d) as compared to IP75-ISO25 showing more distinct phase separation between the bright and dark phases. The phase mixing in IP37.5-ISO62.5 and phase separation in IP75-ISO25 is verified by the absence and presence of the free N—H_2 peak in FTIR spectra (Fig. 2), respectively. A closer look into the phase imaging of IP37.5-ISO62.5 shows a homogeneous dispersion of large aggregates of the soft phase in a pool of continuous bed of hard domains, suggesting that the effect of interurea hydrogen bonding network is more pronounced with the increased hard domain concentration. In contrast, the aggregates of soft phase in IP0-ISO100 and IP75-ISO25 are much smaller in a continuous hard domain bed, which resulted in a higher phase separation degree. Contrary to popular theory, increase in phase separation degree is not necessarily due to increase in bidentate hydrogen bonding formation. Although the phase separation degree of IP75-ISO25 appears to be higher than IP37.5-ISO62.5, it is safe to say the interurea hydrogen bonding in the former is considerably lower as the tensile strength of the composition is lower. The domain size and distribution in the matrix shown in Fig. 4g further validate the tensile and elongation results. The hard domain is largest at IP37.5-ISO62.5 (~16 nm) covering the highest percentage area of 43.58 % resulting in highest resistance to deformation, and thus highest tensile strength. On the other hand, IP75-ISO25 consists of the highest portion of soft domain of 60.32 %, however exhibited lower elongation than IP0-ISO100 due to the isolated soft domain distribution as shown in Fig. 4f. Although the hard domain size for IP0-ISO100 is same as IP75-ISO25, the higher soft domain size in the former surrounds the adjacent urea groups giving higher chain mobility and thus, higher elongation.

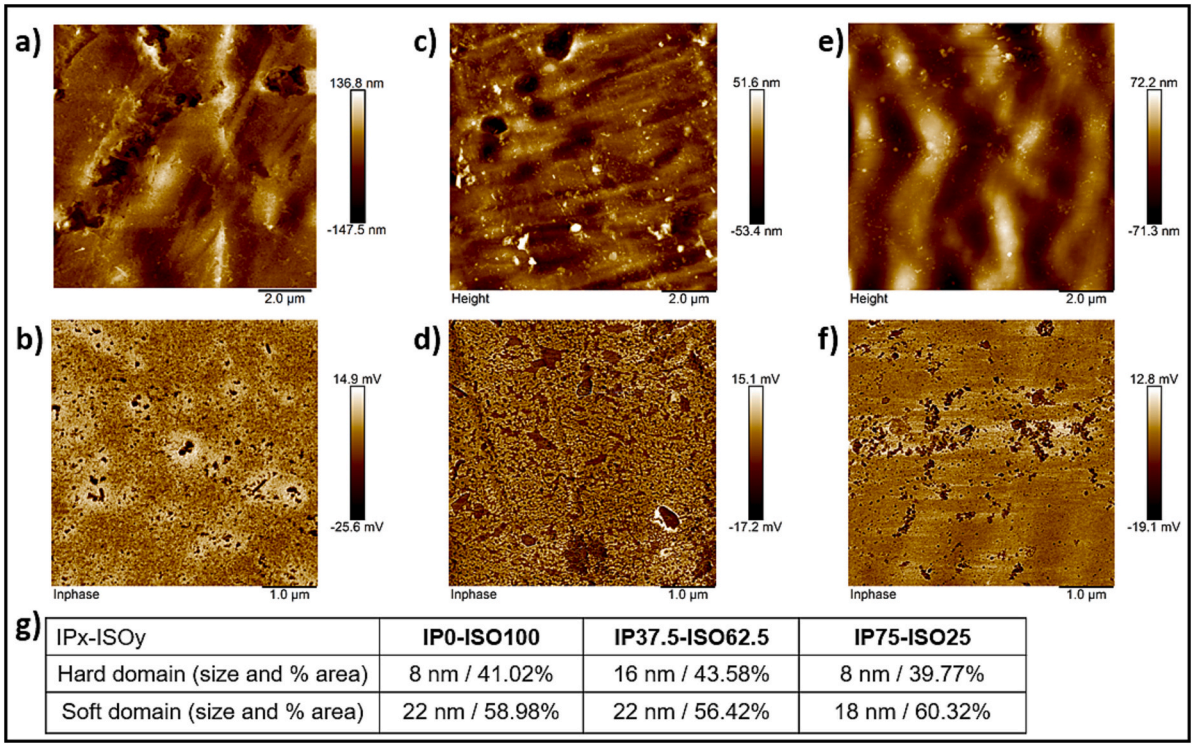

g)

IPx-ISOy	IP0-ISO100	IP37.5-ISO62.5	IP75-ISO25
Hard domain (size and % area)	8 nm / 41.02%	16 nm / 43.58%	8 nm / 39.77%
Soft domain (size and % area)	22 nm / 58.98%	22 nm / 56.42%	18 nm / 60.32%

Fig. 4. ScanAsyst mode AFM height (left) with scan area of 10 µm × 10 µm and phase imaging (right) with a scan area of (5 µm × 5 µm): a) and b) IP0-ISO100; c) and d) IP37.5-ISO62.5; e) and f) IP75-ISO25; g) domain size and distribution.

To complement the AFM images and validate the tensile test results, FESEM was conducted on IPx-ISOy tensile fracture surfaces as shown in Fig. 5. It is important to note that all the tensile specimens are cut in accordance with ISO 37 Type 2 standard with an average gauge width of 3.9 mm. From Fig. 5, the most obvious difference is the width of the specimen after fracture whereby IP0-ISO100 fracture surface appears to be the longest, followed by IP75-ISO25 and then IP37.5-ISO62.5. We could attribute this to the occurrence of plastic deformation to a greater extent for IP0-ISO100 and slightly more for IP75-ISO25. This observation is validated by the lowest elastic modulus and highest elongation at break achieved by IP0-ISO100 as shown in Table 2. Another significant difference in the FESEM images is the fracture behavior of these specimens. IP37.5-ISO62.5 fracture surface exhibits greater and higher contrast of crazes, cracks, and delamination of the polyurea layers making it difficult to determine the exact fracture point of the specimen. This shows that the polyurea chains experienced greater resistance to deformation during tensile loading resulting in the stretching and crazing of the layers. This observation validates the highest tensile strength and highest elastic modulus achieved by IP37.5-ISO62.5. On the other hand, for IP0-ISO100, the fracture appears to have initiated from the macro void on the upper part of the fracture surface and the crack propagated to adjacent macro void and continued across the cross-section. As for IP75-ISO25, no macro voids are visible, and the fracture may have been initiated by nanovoids from one end and propagated across resulting in fine fracture line.

3.4. Surface wettability

Water contact angle (WCA) is an important parameter used to evaluate the surface tension and wettability properties of a coating surface. Fig. 6(a) shows the change in static WCAs of IPx-ISOy films as a function of time. IP37.5-ISO62.5 clearly showed the least surface wettability property as all the lower bound error bars are well above the contact angles of IP0-ISO100 and IP75-ISO25. The WCA for IP37.5-ISO62.5 exhibits significantly highest throughout 270 s and shows a steady decrease over time along with IP75-ISO25. While the WCA for IP0-ISO100 shows very little changes with increasing water contact time. The time dependence of static WCAs is related to the alternating change of up and down (surface reorganization) between non-polar groups and polar groups in aqueous environment. The chain ends of

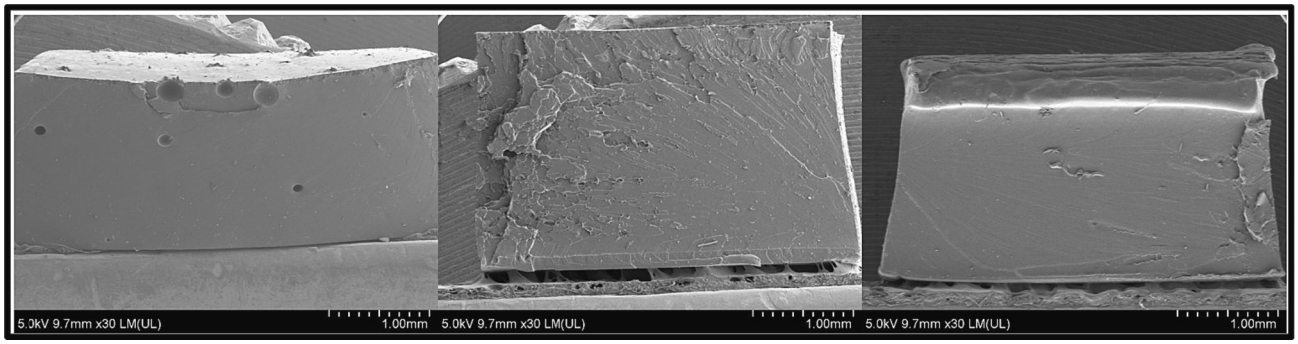

Fig. 5. FESEM images of fracture surface of IPx-ISOy after uniaxial tensile failure at ×30 magnification. From left to right: IP0-ISO100, IP037.5-ISO62.5, IP75-ISO25.

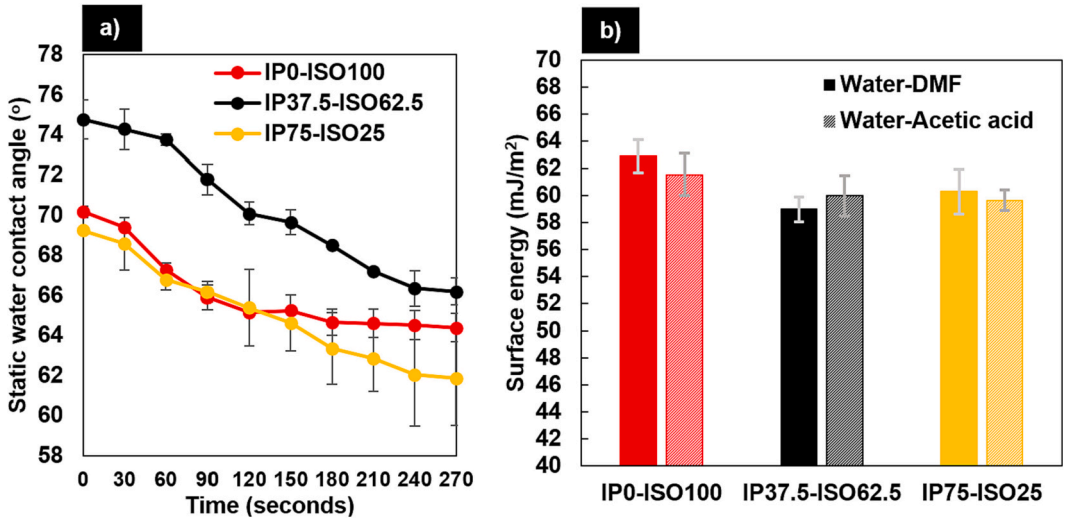

Fig. 6. Surface wettability properties of IPx-ISOy films. a) Static water contact angle evolution over 270 s and b) surface energy of IPx-ISOy films in two systems; water-DMF and water-acetic acid.

the diamine, containing a primary amine and carbonyl group in urea linkages, are extremely polar [56]. This suggests that IP0-ISO100 and IP75-ISO25 contain more unreacted diamines or uncross-linked urea groups on the surface due to their lower WCA. All three films' WCA reached an equilibrium at around 240 s; the equilibrium WCAs are 64.4°, 66.2° and 61.9° for IP0-ISO100, IP37.5-ISO62.5 and IP75-ISO25 respectively, showing an obvious aliphatic isocyanate content dependence reaching peak at 37.5 wt% IPDI.

The initial static WCA behavior of IPx-ISOy films is further studied by determining the surface energy of the films using two polar-nonpolar liquid systems; water-DMF and water-acetic acid. The initial static contact angles (CA) of DMF on the surfaces are in the range 23–30° whereas the initial CAs of acetic acid on the surfaces are higher and constant for all the films at ~43°. Two observations could be stated here; acetic acid is a more stable non-polar liquid than DMF and the CAs of these non-polar liquids are much lower than WCAs due to the high content of non-polar molecules at the surface of the films getting attracted to the testing liquids. The corresponding surface energies of the two systems are shown in Fig. 6(b). It could be seen that the surface reorganization of the polar groups in polyurea matrix did bring some changes in the surface energies of the films but not significantly different from each other. In both IP37.5-ISO62.5 and IP75-ISO25, there are two types of diisocyanates competing for reaction with diamine to form hard segments. The resulting hard segments then compete to form hard domains with each other. The organization of these segments may have been incomplete before the curing of the films such that they brought little differences in the surface energies.

3.5. Thermogravimetric analysis

The thermogravimetric analysis curves of IPx-ISOy in Fig. 7(a) shows the weight (%) of the specimen remaining during heating from room temperature to 600 °C. The thermal degradation starts from 270 and ends at around 420 °C. The thermal degradation characteristic values are shown in Table 3. The extrapolated onset temperature is a characteristic temperature shown for the first mass loss step. It is taken as the point of intersection of the starting-mass baseline and the tangent to the TGA curve at the point of maximum gradient according to the standard ISO 11358-1. It is well known that urethane and urea linkages start degrading above 200 °C although the TGA curves typically do not exhibit any significant mass loss at this temperature [57,58]. In our previous work [7], we found that the first mass loss step of pure aliphatic polyurea starts around 250 °C whereas in the present work, the thermal

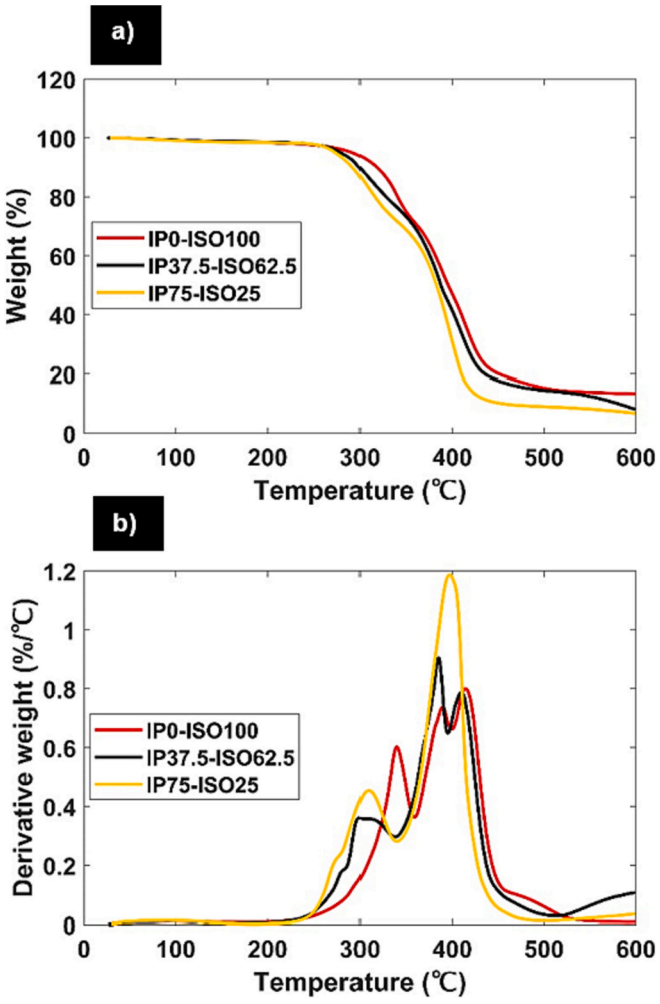

Fig. 7. Thermal degradation properties of IPx-ISOy films. a) TGA curves and b) DTG curves.

degradation of IPx-ISOy starts in the range of 275–323 °C. This result is an indicative that the inclusion of aromatic ring diisocyanate improved the thermal stability of aliphatic polyurea. Looking at the degradation

Table 3
Thermal degradation values of IPx-ISOy films.

Films	Extrapolated onset temperature (°C)	Mass loss in first stage (wt%)	T_{10} (°C)	T_{50} (°C)	T_{90} (°C)	Char residue % at 600 °C
IP0-ISO100	323	29	318	395	>600	13.45
IP37.5-ISO62.5	275	35	299	387	582	8.16
IP75-ISO25	277	39	292	383	468	6.88

pattern, we could see that as the percentage of aliphatic diisocyanate increases, the thermal degradation curve takes a left shift, indicating a decrease in thermal stability. Isophorone diisocyanate is a bulky cyclic aliphatic ring, absent from delocalized π electrons consisting of saturated carbon compound. Hence, it requires lesser energy to break down aliphatic ring structures as compared to aromatic ones.

The degradation steps of segmented polyurea and polyurethane are attributed to their hard and soft segment content [2]. The first degradation temperature is a result of the low thermal stability of urea bonds in the hard segment and the second degradation temperature is attributed to the soft segment covalent bond decomposition. From the TGA curves, the hard segment content for IPx-ISOy is estimated to be in the range of 29 to 39 wt%, the highest for P75-ISO25, whereas the theoretical hard segment is only 30 wt%. This result suggests that inclusion of aliphatic diisocyanates facilitated the formation of hard segments in the matrix. However, contrary to popular belief [59], in this study, aliphatic isocyanates are observed to be thermally less stable than aromatic ones.

Fig. 7(b) presents the gradient of the TGA curve which represents the derivate weight loss per unit temperature. DTG is an important tool to evaluate the stability of the specimen over a range of temperatures and can be used to determine the degrading components at specified temperatures. The DTG curves of IPx-ISOy films presents two obvious peaks, although the second peak for IP0-ISO100 and IP37.5-ISO62.5 are twin peaks. IP75-ISO25 experienced the highest rate of mass loss in both stages at 300 °C and 390 °C, respectively due to the highest content of aliphatic hard segments. One interesting observation is for IP37.5-ISO62.5 specimen, the thermal degradation continues even at temperature above 500 °C as could be seen from the increasing derivative weight loss in this temperature range, whereas for the other two specimens, the derivative weight loss had reached plateau. However, IP0-ISO100 left the greatest char residue at 600 °C, suggesting that aromatic hard and soft segmented polyurea is much stronger and tightly packed, preventing thermal degradation by the hot combustive gases.

3.6. Stress relaxation analysis

Fig. 8(a) demonstrates the amount of stress required to maintain a 0.5 % flexural strain by IPx-ISOy at 80 °C. This trend was determined also at 100 °C for IP37.5-ISO62.5. The test was conducted until each of the specimen reaches a stress plateau, hence the varying duration. The stress relaxation test in this study shows an interesting pattern consisting of two consecutive stages. As concerns stage I, the stress vs time data show a decreasing trend reaching a plateau after a certain time. Then, the stress increases with time reaching a plateau with a value larger than the initial stress. The characteristic values in both the stages at 80 °C are presented in Table 4. The initial stress (s_i) represents the stress value when the specimen is deformed to 0.5 % flexural strain. We detected the highest s_i value for IP37.5-ISO62.5 followed by IP0-ISO100 and then IP75-ISO25. These results complement the 0.2 % offset tensile yield strength trend of the films as shown in Table 2. The relaxation time (t_r), which is the time for the stress to decrease and remain at constant value before the initiation of stage II, is the longest for IP37.5-ISO62.5 and the shortest for IP75-ISO25 as seen in Fig. 8(b). This can be explained by the presence of optimal amount of aliphatic diisocyanate in the former to combine with aromatic diisocyanate forming higher degree of hard

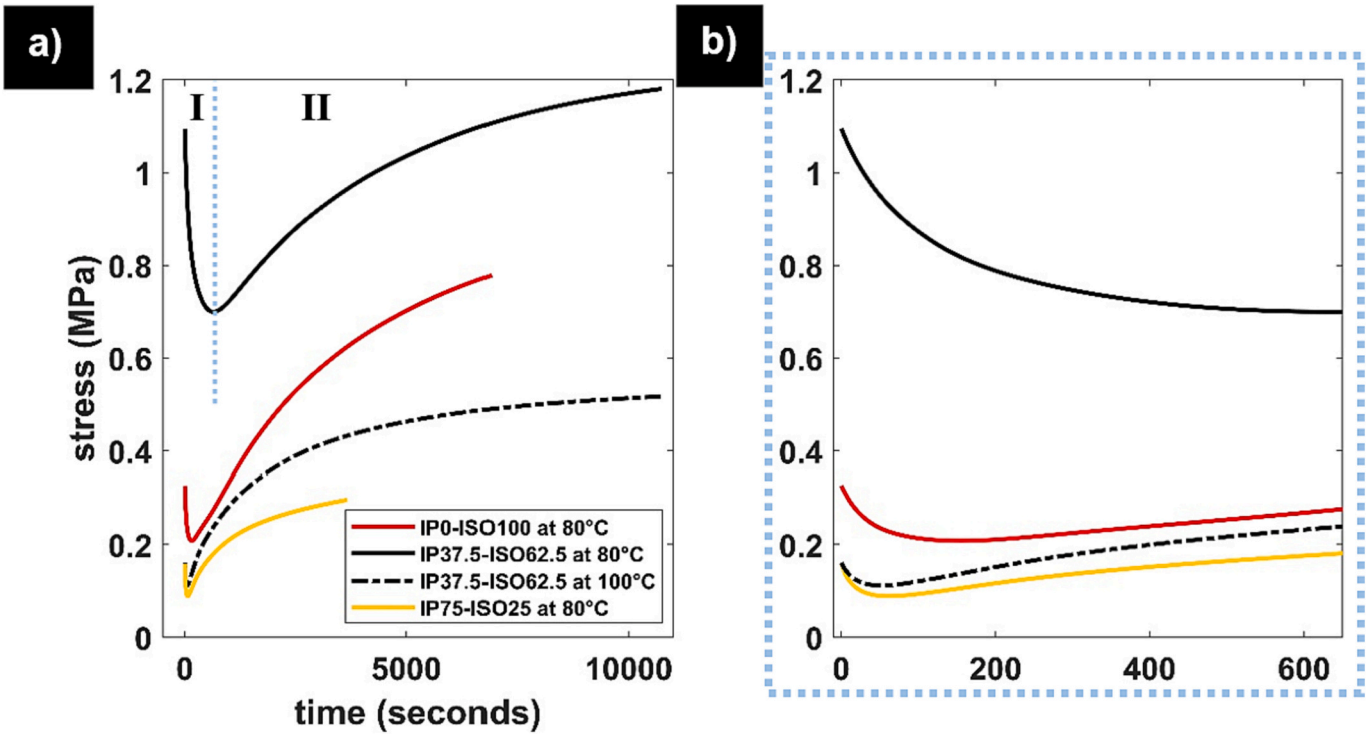

Fig. 8. Stress relaxation curves of IP0-ISO100 at 80 °C, IP37.5-ISO62.5 at 80 °C and 100 °C, IP750-ISO25 at 80 °C under bending mode. a) Full spectra consisting of stage I and stage II as marked on IP37.5-ISO62.5 at 80 °C and b) magnified image of stage I.

Table 4
Stress relaxation test characteristic values for IPx-ISOy at 80 °C.

Films	Stage I			Stage II		
	Initial stress, S_i (kPa)	Stress relaxation rate ($kPas^{-1}$)	Relaxation time, t_r (seconds)	Strain hardening rate ($kPas^{-1}$)	Final stress, S_f (kPa)	t_{S_f} (minutes)
IP0-ISO100	327	−1.41	156	0.01	700	113
IP37.5-ISO62.5	1095	−1.48	646	0.09	1180	171
IP75-ISO25	158	−0.37	62	0.01	300	61

phases that resist deformation greatly as compared to the latter where there is higher amount of aliphatic diisocyanates kinetically mobile and reassemble much faster during constant bending. As for the IP37.5-ISO62.5 at 100 °C, both the s_i and relaxation time (t_r) are very low and short respectively, due to the weakening of the bonds at higher temperatures.

Generally, during stress relaxation, the stress decreases because of breakage of weak bonds such as the hydrogen bond between the urea linkages and then it reaches plateau when all the weak bonds are ruptured leaving only strong bonds which could resist to the deformation. Here, the occurrence of stage II shows that there is not only bond breaking but also bond formation occurring in the polyurea matrix resulting in increase of stress. This could be due to a rearrangement of the polyurea chains, resulting in a re-entanglement which promotes reformation of the hydrogen bonds and in turn increasing dislocations along the matrix [60]. Although stage II did not occur as rapidly as stage I as indicated by the respective phase rate in Table 4, the final stress achieved is higher than the initial stress value. This pattern of stage II is usually observed in time-dependence thermal curing curves for thermoset elastomers and not in stress relaxation of fully cured elastomers. Aromatic polyurea is known to be a thermoset elastomer whereby it hardens and becomes stronger with application of heat. This is because the aromatic diisocyanates contributes to extremely stable covalent crosslinking of hard segments aggregates in the matrix making them extremely difficult to break. As deduced by Holzworth et al. [61], Isonate 143 L contains three arms for crosslinking sites, this case it could increase the chances of re-bonding of hard domains leading to increasing strain hardening rate. From this information, we could hypothesize that the bond rupture in stage I could have left the matrix in a gelation state which forced the urea groups to rebind dynamically and achieve "curing" at the final stress, s_f.

3.7. Cyclic fatigue performance

Fig. 9 shows the stress-fatigue cycle data and power curves fitting for IP0-ISO100, IP37.5-ISO62.5 and IP75-ISO25. Each stress value was based on the peak load upon fracture of each of the composition corresponding to Fig. 3. For all the compositions, the curve fitting begins from the stress value for monotonic tensile values in agreement with the tensile results obtained in Table 2. The number of cycles to failure increases as the the stress applied on the films decreases. As the specimens go through unloading after each cycle, the chains re arrange themselves and there is a relaxation phase through which the stress is redistributed in the matrix. In the case of IP37.5-ISO67.5, at a loading stress of 4.4 MPa (10 % peak load), the specimen sustained up to 5000 cycles without failure. IP0-ISO100 showed the least promising result for fatigue cycles. At lower stress values, the number of cycles was much lower than IP37.5-ISO62.5 and IP0-ISO100. Moreover, the presence of aromatic rings from Isonate 143 L in polyurea chains have also been shown to be stiffer than cycloaliphatic rings of IPDI [62] which causes hindrance on the initial de-entanglement. This affects the chain orientation during unloading after each cycle, whereby the chain may have created more 'knots' (entanglements of chains creating an aggregation at specific points). The continuous loading and unloading leads to more and more dislocations with less flexibility creating a more plastically deformed polymer and chain scission occurs due to breakage in the backbone to finally lead to a faster fracture. On the other hand, IP75-ISO25 exhibits higher fatigue cycles at higher stress as compared to IP37.5-ISO62.5. It

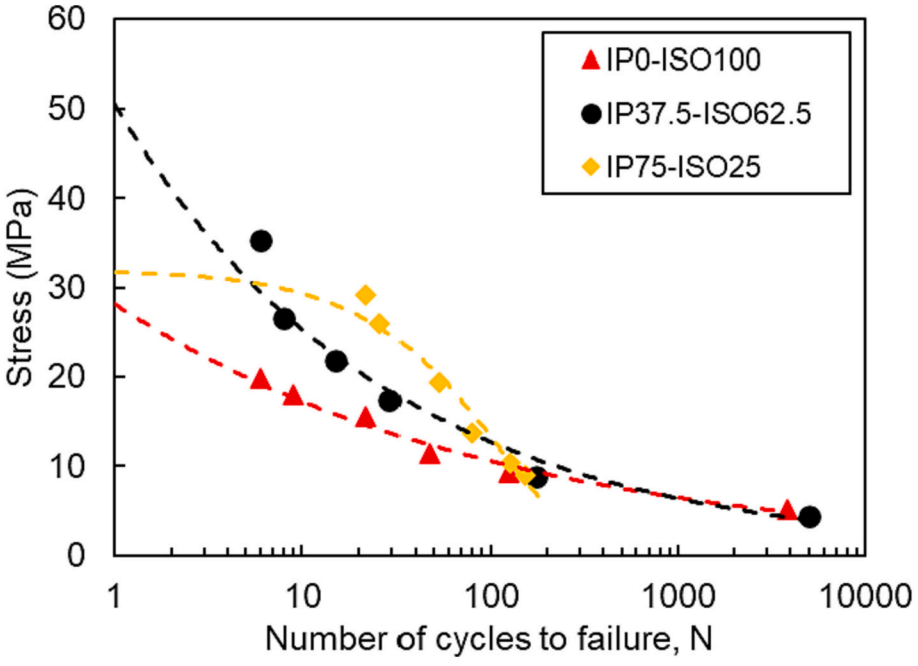

Fig. 9. Stress-number of cycles to failure data with power curve fitting (dashed lines) of IPx-ISOy films.

offers a more flexible, asymmetrical aliphatic structure due to higher percentage of IPDI, or higher steric hindrance [63] and therefore, can go through more cycles at a higher stress.

For IP37.5-ISO62.5, it shows a balance in the steric hindrance and the flexibility of polyurea to absorb the stress. The number of cycles to failure is a balance between 0 % IPDI and 75 % IPDI. This could be due to the more regular orientation of chains within the matrix which creates a more homogenous phase separation of the hard and soft domains. During loading, the elastic region affects the de-entanglement of the soft domains and then as the polymer goes through plastic deformation there is a breakage of the hard domains (breakage of hydrogen bonds between urea linkages). In this case, at lower stress, the polymer goes through a relatively similar number of cycles as IP0-ISO100 due to the de-entanglement and re-entanglement process in the elastic region. However, IP37.5-ISO62.5 can be loaded to higher stress and still goes through the same number of cycles as compared to IP0-ISO100 at lower stress. This could be due to the reduced space between urea linkages by the inclusion of cycloaliphatic IPDI, that allows for a re-formation of hydrogen bonds upon unloading, therefore the strength is retained at the next cycles until microcracks are formed that finally leads to failure. One more possible phenomenon could be associated with the reduced number of cycles for IP37.5-ISO62.5 is that the self-heating of the specimen along the gauge length due to the energy dissipated in the fatigue loading loop as observed by Pichon et al. [64] in their study on thermoplastic polyurethanes. They found that during the initial stages of fatigue cycles, the dissipated energy is lost in the mechanical re-arrangement of the material, and then, as the test progresses, the dissipated energy fully converts into heat softening the material and causing early failure. However, in order to certify these possibilities, further studies on fatigue loading and morphology need to be carried out.

3.8. Anti-corrosion performance

As IP37.5-ISO62.5 showed an exceptional mechanical, thermal and surface wettability behavior, it was chosen to study its anticorrosion performance when it is coated on mild carbon steel plates and exposed in neutral salt spray chamber for extended period. Fig. 10 shows the photographs and optical microscopic images (magnified portion) of IP37.5-ISO62.5 coatings with 0, 14 and 28 days of exposure in the neutral salt spray chamber. Day 7 and Day 21 are excluded in this test as they did not show significant damage to day 0 and day 14 respectively. From the optical images of the coatings on Day 0, it could be seen that

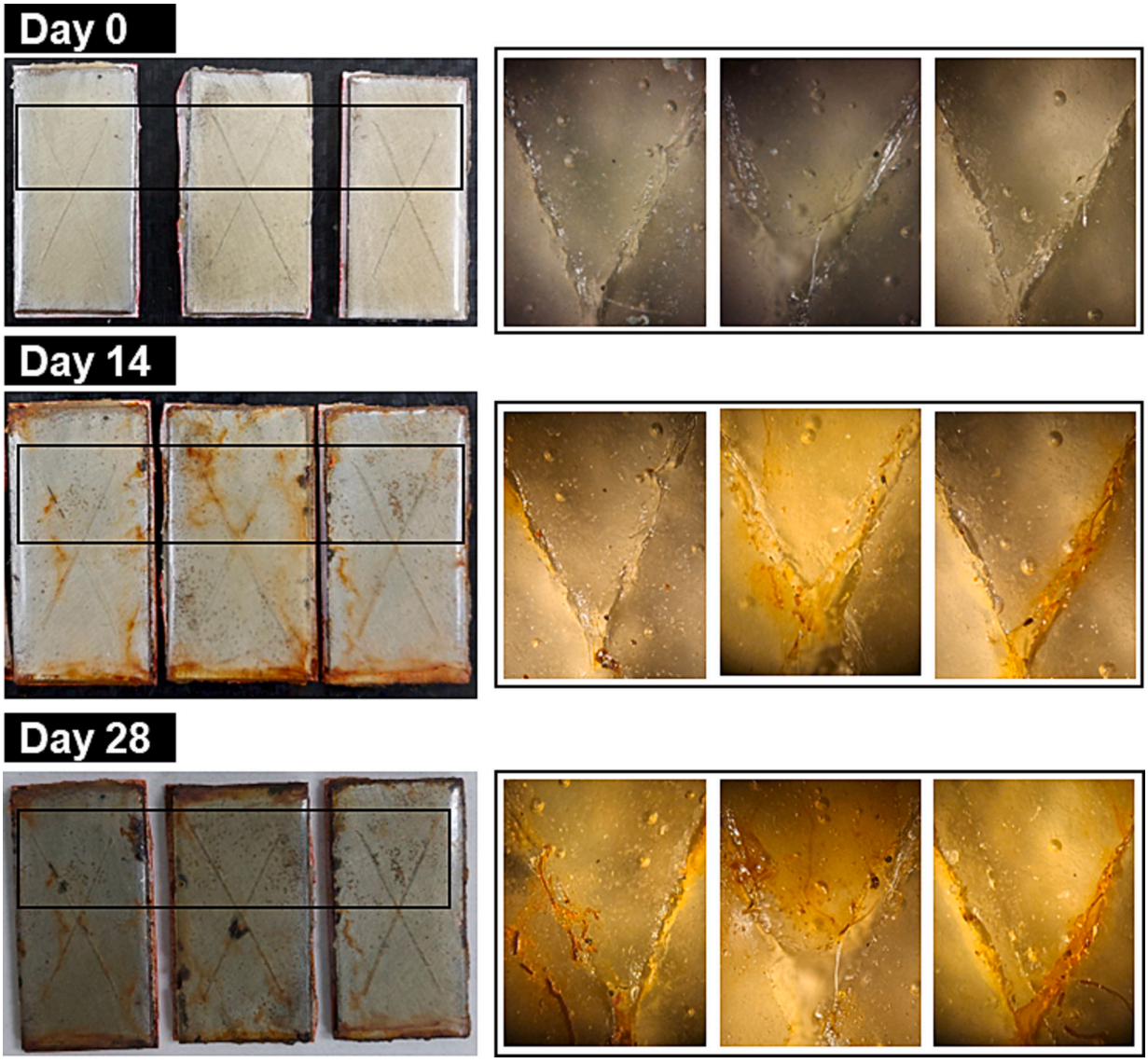

Fig. 10. Visual appearance of three steel plates coated with IP37.5-ISO62.5 after exposure for different periods in neutral salt spray chamber. Left: photographs of the scribed coatings. Right: images taken using optical microscope at ×16 magnification of the upper "cross" region as boxed in the photographs.

the scribe on the coating did not fully expose the underneath steel and the coating looked slightly swollen. This could be due to the dynamic reversible hydrogen bond between the urea groups [65]. For the exposed steel plates, the images show excellent corrosion behavior for ~1.5 mm thick layer cast on steel. The slight corrosion on the border of the coatings visible after 14 days neutral salt spray test duration may be attributed to crevice corrosion starting from the uncoated edges of the steel plates. Slight corrosion is also observed in some parts of the scribe portion under an optical microscope. Pitting corrosion is also observed on the outer area of the scribe which resulted from tiny voids in the coatings. After 28 days of neutral salt spray test duration, both crevice and pitting corrosion grew deeper. Swelling is noticed on the coating in optical image which could be a sign of saltwater penetration into the underneath steel. It is also a sign of the weakening of the coating's adhesion to the steel. The decrease in coating adhesion and increase in swelling is related to the wettability of the coating itself. The higher the wettability, the greater the coating swells and loses adhesion from the substrate. From this study, we see that the coating starts to lose adhesion after 28 days of 3.5 % neutral salt spray in a small part of the specimen. This could be due to various reasons such as non-uniform surface roughness of the substrate prior to coating application, presence of voids resulting from casting method, and seepage of saltwater through the edges of the specimen which is uncoated.

Fig. 11 shows the quantitative effect of neutral salt spray test on the polyurea coating on steel specimens for different exposure durations. The swelling wt% of the coating was determined using the mass change of the coating after exposure in the chamber while it is still in wet condition. The swelling percentage of the coating can be correlated with the saltwater uptake by the coating. As the exposure duration in the chamber increases, the swelling percentage of the coating increases as shown in Fig. 11(a). This could be due to the weakening of the hydrogen bonds between urea groups in constant exposure to corrosive environment, thus giving more space for the penetration of salt ions into the matrix. The weakening of the bonds in the matrix is validated by the decrease in hardness of the coating as shown in Fig. 11(b). Apart from bonding strength and cohesive ability determination, hardness value can also determine the uniformity and curing degree of the coating can judged [45,66]. As the duration of neutral salt spray exposure increases, the coating loses its uniformity which results in weakening of the cohesive forces between the micro segments and gradual decrease in hardness values. From Fig. 11(c), it could be seen that the corrosion growth width increased dramatically after 14 days of exposure, which is a result of accumulation of salt water on the coating surface and possible seepage of the water through voids and defects in the coatings.

4. Conclusion

The influence of aromatic diisocyanate, MDI and aliphatic diisocyanate, IPDI on the mechanical, thermal, surface wettability and stress relaxation behavior of polyurea was investigated. The combination of both these diisocyanates at 37.5 wt% of IPDI resulted in exceptional tensile strength of 47.80 MPa, elastic modulus of 178.57 MPa, and the water contact angle on this surface was the largest at 75°. IP37.5-ISO62.5 showed better properties due to the optimal combination of rigid benzene ring and loosely packed cyclic ring structures to form two different types of hard segments. Both the hard segments increased the cohesive forces between them and strengthened the crosslinking degree between the urea groups. Phase separation degree observations from AFM and failure mechanism observation from FESEM images of the surface and fracture surfaces of IPx-ISOy films, respectively validated the mechanical and thermal results obtained from this study. The stress relaxation test performed at both 80 °C and 100 °C showed the most interesting trend whereby stress decrease and stress increase were noticed over time at constant strain application. For the first time, strain hardening of polyurea was observed during a constant strain application at high temperature. Since IP37.5-ISO62.5 showed an exceptional mechanical behavior, corrosion resistance of this composition was studied on steel specimens. The corrosion resistance study showed that the mixed urea based polyurea coating exhibited excellent corrosion protection efficiency by experiencing swelling and adhesion loss only after 28 days of 3.5 % neutral salt spraying test. This result shows that the designed polyurea coating has excellent protection efficiency in prolonged corrosive environment. Based on the findings of this study, polyurea formulators could selectively combine the advantages of both aliphatic and aromatic diisocyanate structures to design a high-performance polymer as a single coating material and eliminate the

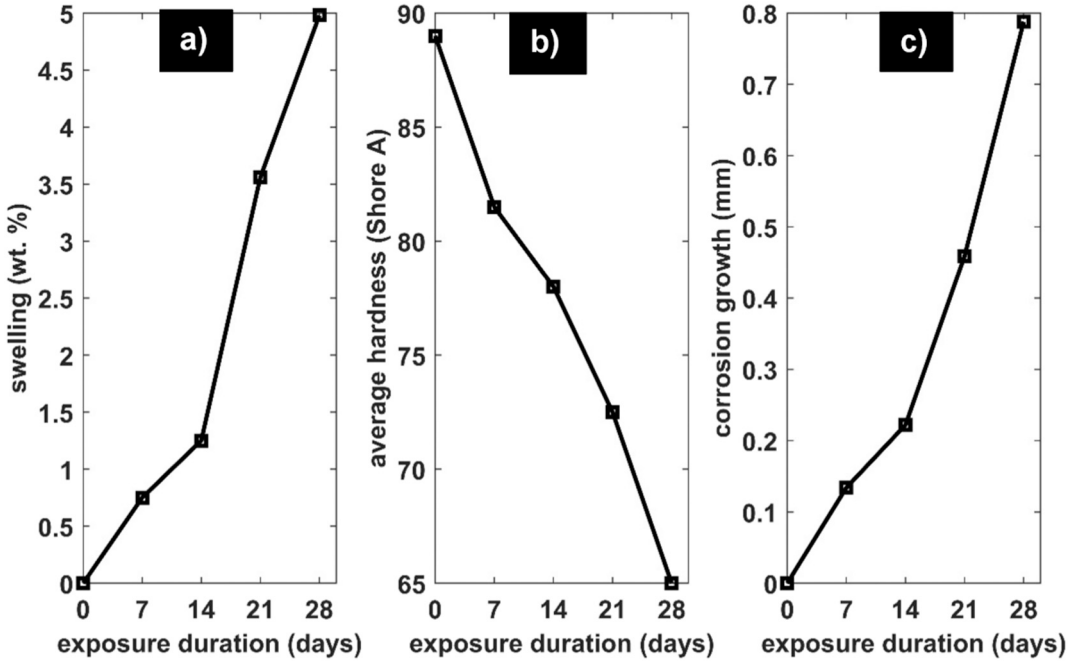

Fig. 11. Effect of 3.5 % neutral salt spray on the IP37.5-ISO62.5 coating on steel specimens for different exposure durations. a) Swelling (wt%), b) average hardness (shore A) and c) corrosion growth (mm).

need for multilayer coating systems.

CRediT authorship contribution statement

Khanisya Palaniandy: Writing – original draft, Visualization, Validation, Methodology, Investigation, Formal analysis, Conceptualization. **Sheik Ambarine Banon Auckloo:** Writing – review & editing, Writing – original draft, Visualization, Investigation. **Giuseppe Cavallaro:** Writing – review & editing, Investigation. **Giuseppe Lazzara:** Writing – review & editing. **Eng-Seng Chan:** Writing – review & editing. **Pooria Pasbakhsh:** Writing – review & editing, Supervision, Conceptualization.

Declaration of competing interest

The authors declare that they have no known competing financial interests or personal relationships that could have appeared to influence the work reported in this paper.

Data availability

The data that has been used is confidential.

Acknowledgements

The authors would like to thank the Ministry of Higher Education Malaysia for providing financial support under the Fundamental Research Scheme, FRGS/1/2018/STG07/MUSM/02/2 and Monash University Malaysia (MUM) for the Ph.D. scholarship. The authors would also like to thank the technical officers of the School of Engineering (MUM) for their assistance and Dr. Mohammad Fahimizadeh for his support throughout this study.

References

[1] O. Rijensky, D. Rittel, Polyurea coated aluminum plates under hydrodynamic loading: does side matter? Int. J. Impact Eng. 98 (2016) 1–12, https://doi.org/10.1016/j.ijimpeng.2016.07.006.
[2] W.H. Awad, C.A. Wilkie, Investigation of the thermal degradation of polyurea: the effect of ammonium polyphosphate and expandable graphite, Polymer (Guildf) 51 (2010) 2277–2285, https://doi.org/10.1016/j.polymer.2010.03.033.
[3] Polyurea: Leading a Revolution in Coating Technology, Paint and Coatings Industry. https://www.pcimag.com/articles/83914-polyurea-leading-a-revolution-in-coating-technology, 2002. (Accessed 17 January 2023).
[4] P. Pasbakhsh, D. Mohotti, K. Palaniandy, S.A.B. Auckloo (Eds.), Polyurea Synthesis, Properties, Composites, Production, and Applications, 1st ed, Elsevier, 2023, https://doi.org/10.1016/C2021-0-01765-X.
[5] D.C.H. Chin, K. Palaniandy, I.L. Hia, P. Pasbakhsh, High performance aliphatic polyurea films reinforced using nonfunctionalized multiwalled carbon nanotubes, Polym. Compos. 41 (2019) 1036–1044, https://doi.org/10.1002/pc.25435.
[6] S.A.B. Auckloo, P. Pasbakhsh, D. Mohotti, Industrial examples of polyurea v/s other polymer coatings, in: P. Pasbakhsh, D. Mohotti, K. Palaniandy, S.A. B. Auckloo (Eds.), Polyurea: Synthesis, Properties, Composites, Production, and Applications, 1st ed, Elsevier, 2023.
[7] K. Palaniandy, S.A.B. Auckloo, G. Cavallaro, E.S. Chan, P. Pasbakhsh, New insights into segmental packing, chain dynamics and thermomechanical performance of aliphatic Polyurea composites: comparison between silica oxides and titanium (III) oxides, Macromol. Mater. Eng. 307 (2021) 2100582, https://doi.org/10.1002/mame.202100582.
[8] X. Li, D. Chen, Synthesis and characterization of aromatic/aliphatic co-polyureas, J. Appl. Polym. Sci. 109 (2008) 897–902, https://doi.org/10.1002/app.24913.
[9] K. Palaniandy, S.A.B. Auckloo, E.-S. Chan, P. Pasbakhsh, Chapter 3 - raw materials, properties, and structure of polyurea, in: P. Pasbakhsh, D. Mohotti, K. Palaniandy, S.A.B. Auckloo (Eds.), Polyurea: Synthesis, Properties, Composites, Production, and Applications, 1st ed, Elsevier, 2023, https://doi.org/10.1016/B978-0-323-99450-7.00005-8.
[10] J. Huang, S. Fu, L. Gan (Eds.), Chapter 8 - Structure, Characterization, and Performance Evaluation of Lignin-Modified Materials, Lignin Chemistry and Applications, Elsevier, 2019, pp. 211–249, https://doi.org/10.1016/B978-0-12-813941-7.00008-4.
[11] S.A.B. Auckloo, Y.M. Hung, P. Pasbakhsh, Synthesis and applications of polyurea composites based on fibers, microfillers and functional materials: a review, in: P. Pasbakhsh, D. Mohotti, K. Palaniandy, S.A.B. Auckloo (Eds.), Polyurea: Synthesis, Properties, Composites, Production, and Applications, 1st ed, Elsevier, 2023.
[12] N. Iqbal, M. Tripathi, S. Parthasarathy, D. Kumar, P.K. Roy, Polyurea coatings for enhanced blast-mitigation: a review, RSC Adv. 6 (2016) 109706–109717, https://doi.org/10.1039/c6ra23866a.
[13] L. Zhang, C. Ji, X. Wang, Y. Wang, G. Wu, H. Zhu, Z. Han, Strengthening and converse strengthening effects of polyurea layer on polyurea–steel composite structure subjected to combined actions of blast and fragments, Thin-Walled Struct. 178 (2022) 109527, https://doi.org/10.1016/j.tws.2022.109527.
[14] M. Grujicic, B.P. d'Entremont, B. Pandurangan, J. Runt, J. Tarter, G. Dillon, Concept-level analysis and design of polyurea for enhanced blast-mitigation performance, J. Mater. Eng. Perform. 21 (2012) 2024–2037, https://doi.org/10.1007/s11665-011-0117-8.
[15] G. Wu, Z. Fang, X. Qin, J. Fu, Preparation and properties of impact resistant polyurea coating for fluorochemical pipeline, Processes 10 (2022), https://doi.org/10.3390/pr10020193.
[16] V. Orlov, Computer simulation of optimal thickness of polyurea coating using for trenchless renovation of potable water pipes, Procedia Eng 165 (2016) 1168–1175, https://doi.org/10.1016/j.proeng.2016.11.835.
[17] S. Bordbar, M. Rezaeizadeh, A. Kavian, Improving thermal conductivity and corrosion resistance of polyurea coating on internal tubes of gas heater by nano silver, Prog Org Coat 146 (2020) 105722, https://doi.org/10.1016/j.porgcoat.2020.105722.
[18] K. Palaniandy, M. Makaremi, P. Pasbakhsh, Chapter 7 - polyurea nanocomposites: synthesis, functional properties, and applications, in: P. Pasbakhsh, D. Mohotti, K. Palaniandy, S.A.B. Auckloo (Eds.), Polyurea: Synthesis, Properties, Composites, Production, and Applications, 1st ed, Elsevier, 2023, https://doi.org/10.1016/B978-0-323-99450-7.00022-8.
[19] Y. Huang, H. Yan, M. Cai, S. Song, C. He, X. Fan, M. Zhu, Polyurea as a reinforcing filler for the anti-corrosion and wear-resistant application of epoxy resin, Prog. Org. Coat. 171 (2022) 107049, https://doi.org/10.1016/j.porgcoat.2022.107049.
[20] H. Beiki, S.J. Mosavi, Silver nanoparticles-polyurea composite coatings on ASTM A194 steel: a study of corrosion behavior in chloride medium, J Bio Tribocorros 6 (2020), https://doi.org/10.1007/s40735-020-00364-9.
[21] W. Funke, How organic coating systems protect against corrosion, in: Polymeric Materials for Corrosion Control, American Chemical Society, 1986, pp. 222–228, https://doi.org/10.1021/bk-1986-0322.ch020.
[22] X. Yuan, Y. Du, B. Lei, Effect of tensile stress on the corrosion performance of silicone-epoxy coatings on 2024 Al-alloy, Mater Today Commun 31 (2022) 103527, https://doi.org/10.1016/j.mtcomm.2022.103527.
[23] L. Feng, J.O. Iroh, Corrosion resistance and lifetime of polyimide-b-polyurea novel copolymer coatings, Prog Org Coat 77 (2014) 590–599, https://doi.org/10.1016/j.porgcoat.2013.11.023.
[24] K. Palaniandy, S.A.B. Auckloo, E.-S. Chan, P. Pasbakhsh, Chapter 1 - formulations and properties: comparative review of aromatic polyurea versus aliphatic polyurea, in: P. Pasbakhsh, D. Mohotti, K. Palaniandy, S.A.B. Auckloo (Eds.), Polyurea: Synthesis, Properties, Composites, Production, and Applications, 1st ed, Elsevier, 2023, https://doi.org/10.1016/B978-0-323-99450-7.00011-3.
[25] K.W. Ng, K.H. Lee, K. Palaniandy, P. Pasbakhsh, Chapter 8 - ultraviolet (UV) resistivity of polyurea composites, in: P. Pasbakhsh, D. Mohotti, K. Palaniandy, S.A. Banon Auckloo (Eds.), Polyurea, Elsevier, 2023, pp. 131–154, https://doi.org/10.1016/B978-0-323-99450-7.00009-5.
[26] S. Das, D.F. Cox, G.L. Wilkes, D.B. Klinedinst, I. Yilgor, E. Yilgor, F.L. Beyer, Effect of symmetry and H-bond strength of hard segments on the structure-property relationships of segmented, nonchain extended polyurethanes and polyureas, J. Macromol. Sci., Part B: Phys. 46 (2007) 853–875.
[27] E. Yildirim, M. Yurtsever, The role of diisocyanate and soft segment on the intersegmental interactions in urethane and urea based segmented copolymers: a DFT study, Comput. Theor. Chem. 1035 (2014) 28–38, https://doi.org/10.1016/j.comptc.2014.02.021.
[28] Y. He, X. Zhang, J. Runt, The role of diisocyanate structure on microphase separation of solution polymerized polyureas, Polymer (Guildf) 55 (2014) 906–913, https://doi.org/10.1016/j.polymer.2014.01.001.
[29] Y. He, D. Xie, X. Zhang, The structure, microphase-separated morphology, and property of polyurethanes and polyureas, J. Mater. Sci. 49 (2014) 7339–7352, https://doi.org/10.1007/s10853-014-8458-y.
[30] S. Sami, E. Yildirim, M. Yurtsever, E. Yurtsever, E. Yilgor, I. Yilgor, G.L. Wilkes, Understanding the influence of hydrogen bonding and diisocyanate symmetry on the morphology and properties of segmented polyurethanes and polyureas: computational and experimental study, Polymer (Guildf) 55 (2014) 4563–4576.
[31] J.P. Sheth, D.B. Klinedinst, G.L. Wilkes, I. Yilgor, E. Yilgor, Role of chain symmetry and hydrogen bonding in segmented copolymers with monodisperse hard segments, Polymer (Guildf) 46 (2005) 7317–7322.
[32] T. Li, T. Zheng, J. Han, Z. Liu, Z.X. Guo, Z. Zhuang, J. Xu, B.H. Guo, Effects of diisocyanate structure and disulfide chain extender on hard segmental packing and self-healing property of polyurea elastomers, Polymers (Basel) 11 (2019), https://doi.org/10.3390/polym11050838.
[33] K. Kojio, S. Nakashima, M. Furukawa, Microphase-separated structure and mechanical properties of norbornane diisocyanate-based polyurethanes, Polymer (Guildf) 48 (2007) 997–1004, https://doi.org/10.1016/j.polymer.2006.12.057.
[34] Y. Wang, L. Wang, H. Liu, S. He, X. Liu, W. Liu, M. Huang, C. Zhu, Polyurethane as smart biocoatings: effects of hard segments on phase structures and properties, Prog Org Coat 150 (2021) 106000, https://doi.org/10.1016/j.porgcoat.2020.106000.
[35] M. Hoorfar, A.W. Neumann, Axisymmetric drop shape analysis (ADSA) for the determination of surface tension and contact angle, J Adhes 80 (2004) 727–743, https://doi.org/10.1080/00218460490477684.

[36] N. Iqbal, M. Tripathi, S. Parthasarathy, D. Kumar, P.K. Roy, Tuning the properties of segmented polyurea by regulating soft-segment length, J. Appl. Polym. Sci. 135 (2018) 46284.
[37] D.J. Kinning, Bulk, surface, and interfacial characterization of silicone - Polyurea segmented copolymers, J. Adhes. 75 (2001) 1–26, https://doi.org/10.1080/00218460108029591.
[38] Y. Li, W. Kang, J.O. Stoffer, B. Chu, Effect of hard-segment flexibility on phase separation of segmented polyurethanes, Macromolecules 27 (1994) 612–614.
[39] S. Das, I. Yilgor, E. Yilgor, B. Inci, O. Tezgel, F.L. Beyer, G.L. Wilkes, Structure–property relationships and melt rheology of segmented, non-chain extended polyureas: effect of soft segment molecular weight, Polymer (Guildf) 48 (2007) 290–301.
[40] N. Iqbal, M. Tripathi, S. Parthasarathy, D. Kumar, P.K. Roy, Polyurea spray coatings: tailoring material properties through chemical crosslinking, Prog Org Coat 123 (2018) 201–208, https://doi.org/10.1016/j.porgcoat.2018.07.005.
[41] H. Huang, H. Pang, J. Huang, P. Yu, J. Li, M. Lu, B. Liao, Influence of hard segment content and soft segment length on the microphase structure and mechanical performance of polyurethane-based polymer concrete, Construct. Build Mater. 284 (2021) 122388, https://doi.org/10.1016/j.conbuildmat.2021.122388.
[42] J. Zheng, R. Ozisik, R.W. Siegel, Phase separation and mechanical responses of polyurethane nanocomposites, Polymer (Guildf) 47 (2006) 7786–7794, https://doi.org/10.1016/j.polymer.2006.08.068.
[43] A.M. Castagna, A. Pangon, T. Choi, G.P. Dillon, J. Runt, The role of soft segment molecular weight on microphase separation and dynamics of bulk polymerized polyureas, Macromolecules 45 (2012) 8438–8444, https://doi.org/10.1021/ma3016568.
[44] Y. Li, W. Kang, J.O. Stoffer, B. Chu, Effect of hard-segment flexibility on phase separation of segmented polyurethanes, Macromolecules 27 (1994) 612–614, https://doi.org/10.1021/ma00080a043.
[45] J. Yan, Z. Gao, J. Song, Z. Liu, Q. Tan, Corrosion behavior of carbon nanotubes/polyurea composite coatings in alkaline environment, Int. J. Electrochem. Sci. 15 (2020) 10253–10261.
[46] Y. Li, B. Luo, C. Guet, S. Narasimalu, Z. Dong, Preparation and formula analysis of anti-biofouling titania–polyurea spray coating with nano/micro-structure, Coatings 9 (2019) 560, https://doi.org/10.3390/coatings9090560.
[47] Y. Li, Y. Woo, M. Sekar, S. Narasimalu, Z. Dong, Effect of nano-titanium dioxide contained in titania-polyurea coating on marina biofouling and drag reduction, J. Biomed. Nanotechnol. 16 (2020) 1530–1541, https://doi.org/10.1166/jbn.2020.2980.
[48] Z. Rong, Y. Li, R.Z. Lim, H. Wang, Z. Dong, K. Li, X. Wang, Fire-retardant effect of titania-polyurea coating and additional enhancement via aromatic diamine and modified melamine polyphosphate, Npj Mater Degrad 6 (2022) 38, https://doi.org/10.1038/s41529-022-00248-y.
[49] B. Lucio, J.L. de la Fuente, Catalytic effects over formation of functional thermoplastic elastomers for rocket propellants, Polym. Adv. Technol. 33 (2022) 807–817, https://doi.org/10.1002/pat.5557.
[50] H. Ma, Y. Liu, T. Chai, Y. Yu, J. Guo, L. Zhong, Q. Zhang, The effect of single curing agents on the curing reactions of the HTPB-based binder system, Coatings 12 (2022) 1090.
[51] N.H. Mudri, L.C. Abdullah, M.M. Aung, M.Z. Salleh, D.R. Awang Biak, M. Rayung, Comparative study of aromatic and cycloaliphatic isocyanate effects on physico-chemical properties of bio-based polyurethane acrylate coatings, Polymers (Basel) 12 (2020) 1494.
[52] M.S. Dongyu Cai, High mechanical performance polyurea/organoclay nanocomposites, Compos. Sci. Technol. 103 (2014) 44–48.
[53] M.H. Kirmani, P.J. Arias-Monje, S. Kumar, High interfacial shear strain in polyurea-carbon nanotube composite sheets, ACS Appl Nano Mater 2 (2019) 6849–6857, https://doi.org/10.1021/acsanm.9b01291.
[54] H. Haddadi, E. Nazockdast, B. Ghalei, Chemorheological characterization of thermosetting polyurethane formulations containing different chain extender contents, Polym. Eng. Sci. 48 (2008) 2446–2453, https://doi.org/10.1002/pen.21229.
[55] S.A. Shokry, A.K. El Morsi, M.S. Sabaa, R.R. Mohamed, H.E. El Sorogy, Synthesis and characterization of polyurethane based on hydroxyl terminated polybutadiene and reinforced by carbon nanotubes, Egypt. J. Pet. 24 (2015) 145–154, https://doi.org/10.1016/j.ejpe.2015.05.008.
[56] D. Fragiadakis, R. Gamache, R.B. Bogoslovov, C.M. Roland, Segmental dynamics of polyurea: effect of stoichiometry, Polymer (Guildf) 51 (2010) 178–184, https://doi.org/10.1016/j.polymer.2009.11.028.
[57] K. Palaniandy, S.A.B. Auckloo, P. Pasbakhsh, Chapter 4 - relationship between performance and properties of polyurea through different synthesis protocols: a review of different case studies, in: P. Pasbakhsh, D. Mohotti, K. Palaniandy, S.A. B. Auckloo (Eds.), Polyurea: Synthesis, Properties, Composites, Production, and Applications, 1st ed, Elsevier, 2023, https://doi.org/10.1016/B978-0-323-99450-7.00018-6.
[58] T. Hentschel, H. Münstedt, Kinetics of the molar mass decrease in a polyurethane melt: a rheological study, Polymer (Guildf) 42 (2001) 3195–3203, https://doi.org/10.1016/S0032-3861(00)00489-4.
[59] F.M.B. Coutinho, M.C. Delpech, T.L. Alves, A.A. Ferreira, Degradation profiles of cast films of polyurethane and poly(urethane-urea) aqueous dispersions based on hydroxy-terminated polybutadiene and different diisocyanates, Polym. Degrad. Stab. 81 (2003) 19–27, https://doi.org/10.1016/S0141-3910(03)00058-2.
[60] S.A.B. Auckloo, K. Palaniandy, Y.M. Hung, G. Lazzara, S.P. Chai, P. Pasbakhsh, Nonporous, strong, stretchable, and transparent electrospun aromatic polyurea nanocomposites as potential anticorrosion coating films, Nanomaterials 11 (2021), https://doi.org/10.3390/nano11112998.
[61] Z.J.K. Holzworth, A.V. Amirkhizi, J. Qiao, S. Nemat-Nasser, Effect of isocyanate content on thermal and mechanical properties of polyurea, Polymer (Guildf) 54 (2013) 3079–3085.
[62] N. Iqbal, M. Tripathi, S. Parthasarathy, D. Kumar, P.K. Roy, Aromatic versus aliphatic: hydrogen bonding pattern in chain-extended high-performance polyurea, Chemistry Select 3 (2018) 1976–1982, https://doi.org/10.1002/slct.201703176.
[63] N.H. Mudri, L.C. Abdullah, M.M. Aung, M.Z. Salleh, D.R. Awang Biak, M. Rayung, Comparative study of aromatic and cycloaliphatic isocyanate effects on physico-chemical properties of bio-based polyurethane acrylate coatings, Polymers (Basel) 12 (2020), https://doi.org/10.3390/polym12071494.
[64] P.G. Pichon, M. Boutaous, F. Méchin, H. Sautereau, Measurement and numerical simulation of the self heating of cross-linked segmented polyurethanes under cyclic loading, Eur. Polym. J. 48 (2012) 684–695, https://doi.org/10.1016/j.eurpolymj.2012.01.005.
[65] V. Alizadeh, A.V. Amirkhizi, Thermo-mechanical characterization of polyurea hybrid blend variants, in: M. Silberstein, A. Amirkhizi, X. Shuman, A. Beese, R. B. Berke, G. Pataky (Eds.), Challenges in Mechanics of Time Dependent Materials, Fracture, Fatigue, Failure and Damage Evolution Vol. 2, Springer International Publishing, Cham, 2020, pp. 163–166.
[66] J.C. Wong, K.H. Ngoi, C.H. Chia, T. Jeon, H. Kim, H.-J. Kim, H.-C. Kim, M. Ree, Surface hardness and abrasion resistance natures of thermoplastic polymer covers and windows and their enhancements with curable tetraacrylate coating, Polymer (Guildf) 239 (2022) 124419, https://doi.org/10.1016/j.polymer.2021.124419.